River Flow 2010 - Dittrich, Koll, Aberle & Geisenhainer (eds) - © 2010 Bundesanstalt für Wasserbau ISBN 978-3-939230-00-7

Description of the idealized bed roughness effects on tracer transport in water flumes by applying the strange attractor multifractal analysis

F.J. Jimenez-Hornero & E. Gutierrez de Rave
Department of Graphic Engineering and Geomatics, University of Cordoba, Spain

T. Vanwalleghem & J.V. Giraldez
IAS CSIC and Department of Agronomy, University of Cordoba, Spain

J.E. Jimenez-Hornero
Department of Computing and Numerical Analysis, University of Cordoba, Spain

A.M. Laguna
Department of Applied Physics, University of Cordoba, Spain

ABSTRACT: A numerical simulation of the skimming and wake interference flows due to the influence of an idealized bed roughness in a water flume was carried out using the lattice model approach. The model reproduced the skimming and wake interference regimes for different aspect ratios that determine the bed roughness geometry. The simulated turbulent structures were visualized by drawing the trajectories of a large number of passive tracer particles released in the computational domain. The strange attractor multifractal formalism has been used here with the aim of analysing the time series in the tracer transport for the simulated flows. The results obtained from a study of the mass exponent functions showed the multifractal nature of the tracer transport for both flow regimes. Multifractal spectra confirmed heterogeneity in the time series as well as the presence of extreme high values for the skimming flow as a consequence of the turbulence intensity. The detailed information on the time series structure provided by the multifractal analysis demonstrated the potential of this approach for describing pollutant and sediment dispersion in turbulent open channel flows.

Keywords: multifractal analysis; skimming flow, wake interference flow, tracer transport

1 INTRODUCTION

The bed roughness geometry has a major influence on the turbulence production in the boundary layer causing different flow regimes, as has been shown in many works (e.g. Perry & Joubert, 1963; Grass, 1971; Cui et al., 2003). The flow regime classification proposed by Morris (1955) can be adopted in hydraulic engineering to study the influence of the bed roughness geometry on the turbulent flow in a water flume(e.g. Khan et al., 2005). Thus, by using the so-called aspect ratio h/w, with h and w being the height of the roughness element and the gap distance that separates two of those elements, respectively, to describe three flow regimes: a) isolated roughness flow when the roughness elements are well separated ($h/w < 0.3$); b) wake interference flow when the disturbed flow does not have enough distance between obstacles to reorganize itself ($h/w \approx 0.5$); and c) skimming flow characterised by the formation of a single vortex within each cavity as a consequence of a small separation between roughness elements ($h/w \approx 1$).

Khan et al. (2005) investigated the transition between the skimming and wake interference flows using aspect ratios of 0.67 and 0.5 for an idealized bed roughness, whose elements were placed in a water flume of 6.2 m in length, 0.5 m in width and 0.3 m in height. The roughness elements were formed from lengths of a 5×10^{-3} m square brass bar. Khan et al. (2005) used Rhodamine-6G and water-soluble Nigrosine crystals as tracer dyes to visualize the turbulent structures. These authors found that the wake interference flows was associated with an increase in the turbulence production in the boundary layer, which caused a greater dispersion of the dye tracer inside the cavities, and a reduction in shear at the top of the roughness elements.

With the aim of obtaining an increased knowledge of the influence of the skimming and wake interference flows on passive tracer transport time series, the coupling of the lattice Bhatnagar-Gross-Krook (BGK) (e.g. Succi, 2001), Smagorinsky eddy viscosity (e.g. Pope, 2000) and flow visualization (Xia & Leung, 2001) models, used to simulated the conditions reported by Khan et al.

(2005), with the strange attractor multifractal formalism (Hentschel & Procaccia, 1983; Grassberger, 1983; Halsey et al., 1986) is used in this work. The lattice BGK model is a numerical integration of the Navier-Stokes equations proposed by Chen et al. (1992) and Qian et al. (1992). It is based on a simplification of the lattice Boltzmann (LB) equation (Succi, 2001). Thus, the lattice BGK model shares the features of the LB method, which can be classified as an explicit, Lagrangian, finite-hyperbolicity approximation of the Navier-Stokes equations. It is frequent the use of the LB method for dealing with problems of interest to the hydraulic engineering community involving turbulent flows (Zhou, 2002) by applying, in these cases, the large eddy simulation (LES) scheme that can describe turbulence in any dimension although it was developed for 3D flows (Pope, 2000; Davidson, 2004).

2 METHODS

2.1 *Simulation of time series in passive tracer transport*

In the lattice BGK model, the fluid particles move in a regular lattice, in which each node is linked to its neighbours following a vicinity model that is chosen depending on the complexity of the phenomenon to be simulated. The vicinity model *d2q9* is used to calculate the fluid velocity field in two dimensions (e.g. Succi, 2001), with $d = 2$ meaning the number of dimensions and $q = 9$ the number of particles considered. In this case, there are eight moving particles and one at rest. The independent variable f_i varies continuously between 0 and 1 according to the Boltzmann molecular chaos hypothesis and represents the probability of finding a fluid particle in a link i that connects a node with one of its neighbours. The interactions of the particles keep up the mass and momentum (Chopard & Droz, 1998). The equation of the lattice BGK model for a node $\mathbf{r}$ at time t, is (Succi, 2001)

$$f_i\left(\mathbf{r}+\mathbf{c}_i,t+1\right)=\frac{1}{\eta}f_i^{\mathrm{eq}}\left(\mathbf{r},t\right)+\left(1-\frac{1}{\eta}\right)f_i\left(\mathbf{r},t\right) \quad (1)$$

where $\mathbf{c}_i$ is the velocity vector of a fluid particle in the link i, f_i^{eq} is the local equilibrium function and η is the relaxation time parameter that represents the difference between f_i and f_i^{eq}. Using the Chapman-Enskog expansion, it is mathematically demonstrable that Eq. (1) can recover the Navies-Stokes equations to the second order of accuracy (Chen & Doolen, 1998) if f_i^{eq} is chosen in the following way:

$$f_i^{\mathrm{eq}}=\rho\mu_i\left[1+\frac{c_{i\alpha}u_\alpha}{c_s^2}+\frac{1}{2}\left(\frac{c_{i\alpha}u_\alpha}{c_s^2}\right)^2-\frac{u_\alpha u_\alpha}{2c_s^2}\right] \quad (2)$$

where the Einstein summation convention has been adopted and α represents the spatial coordinates, x and z. The parameter c_s is selected according to the vicinity model chosen and the μ_i's are weighting factors associated with the lattice directions. $\rho\left(\mathbf{r},t\right)=\sum_{i=0}^{q-1}f_i\left(\mathbf{r},t\right)$ and $\mathbf{u}\left(\mathbf{r},t\right)=\sum_{i=1}^{q-1}f_i\left(\mathbf{r},t\right)\mathbf{c}_i\Big/\rho\left(\mathbf{r},t\right)$ stand for the fluid density and velocity, respectively. The relaxation time parameter determines the kinematic viscosity $\upsilon=c_s^2\left(\eta-0.5\right)$.

In the case of the simulation of turbulent flows, it is possible to use the LES scheme within the lattice BGK model. According to Hou et al. (1996), the essential idea of LES, based on the smoothing of the flow velocity by applying a convolution with a filter, can be included in the lattice BGK model as a spatially-dependent effective viscosity $\tilde{\upsilon}=\upsilon+\upsilon_t$, made up of υ and an eddy viscosity υ_t. The eddy viscosity is determined by using the Smagorinsky eddy viscosity model (Pope, 2000). Thus, a spatially-dependent relaxation time $\tilde{\eta}=0.5\left(\eta+\left(\eta^2+2C_{smg}^2\left(\left(\Pi_{xz}\Pi_{xz}\right)^{0.5}\Big/\rho\right)\right)^{0.5}\right)$ is obtained, with $\Pi_{xz}=\sum_{i=1}^{q-1}c_{ix}c_{iz}\left(f_i-f_i^{\mathrm{eq}}\right)$ as the non-equilibrium momentum flux tensor (Chopard & Droz, 1998) and C_{smg} being the Smagorinsky constant. $\tilde{\eta}$ substitutes η in Eq. (1) allowing the calculation of the filtered fluid density and velocity. The original Smagorinsky model is too dissipative in the presence of a wall (Davidson, 2004) when the "universal" or Lilly-Smagorinsky constant, C_{smg} = 0.17-0.18, is used. However, most researchers prefer C_{smg} = 0.1-0.12 (Lesieur et al., 2005) as has been assumed in this work. Thus, the Smagorinsky model behaves well for free-shear flows, wall flows with wall laws and channel flows (e.g. Davidson, 2004) at relatively low Reynolds numbers (Re = 2000-10000).

In order to visualize the simulated flow regime, the trajectories of the released passive tracer particles were determined by using a method based on that proposed by Xia & Leung (2001). Thus, at each time step Δt, the position $\mathbf{r}_p$ of a particle was calculated from $\mathbf{r}_p(t+\Delta t) = \mathbf{r}_p(t) + \mathbf{u}'\Delta t$, where the velocity $\mathbf{u}'$ was derived by applying a bilinear interpolation to the instantaneous velocity field obtained with the lattice BGK model, $\mathbf{u}$.

2.2 *Multifractal analysis*

The strange attractor multifractal formalism was used to perform the multifractal analysis on the simulated time series in the tracer transport. In order to apply this formalism, the series were divided into non-overlapping intervals of a certain time resolution, δ. Thus, δ and the amount of tracer particles, c_i, characterized each interval i. The minimum time resolution, δ_{ini}, was chosen so that every initial interval contained at least one non-zero value of the amount of tracer particles, c_{ini}. c_i was set to be equal to this value or to the average if there were several values in every initial interval. Thus, the probability mass function $c_i(\delta)$ at time resolution δ is defined in each interval i as (e.g. Kravchenko et al., 1999)

$$c_i(\delta) = \frac{c_i}{\sum_{j=1}^{n_{ini}} (c_{ini})_j} \tag{3}$$

where c_i is calculated based on the c_{ini} values and n_{ini} is the number of initial intervals of time resolution δ_{ini}. The distribution of the probability mass function was analyzed by using the method of moments (Evertsz & Mandelbrot, 1992), in which the partition function $\chi(q,\delta)$ of order q is calculated from the $c_i(\delta)$ values:

$$\chi(q,\delta) = \sum_{i=1}^{n} \left[c_i(\delta) \right]^q \tag{4}$$

with n being the number of intervals of time resolution δ and $q \in]-\infty,\infty[$. The partition function has the following scaling property for a multifractal measure

$$\chi(q,\delta) \approx \delta^{\tau(q)} \tag{5}$$

where $\tau(q)$ is a non-linear function of q and is known as the mass exponent function. For each q, $\tau(q)$ can be obtained as the slope of the linear segment of a log-log plot of $\chi(q,\delta)$ versus δ. For $q >> 1$, the value of $\chi(q,\delta)$ is mainly determined by the high data values, while the influence of the low data values contributes most to the partition function for $q << -1$ (Kravchenko et al., 1999). The Lipschitz-Hölder or singularity exponent α quantifies the strength of the measure singularities. Its value is found from the scaling relation $c_i(\delta) \approx \delta^{\alpha}$, when $\delta \to 0$. α is also known as the local fractal dimension and can be determined by Legendre transformation of the $\tau(q)$ curve (Evertsz & Mandelbrot, 1992):

$$\alpha(q) = \frac{d\tau(q)}{dq} \tag{6}$$

Let $N(\alpha,\delta)$ be the number of intervals of a given time resolution δ, where a given value of α is found, and define $f(\alpha)$ from the scaling relation:

$$N(\alpha,\delta) \approx \delta^{-f(\alpha)} \tag{7}$$

$f(\alpha)$ can be considered as the fractal dimension of the set of intervals that corresponds to a singularity α. A plot of $f(\alpha)$ versus α is called the multifractal spectrum. $f(\alpha)$ can be calculated from (Chhabra & Jensen, 1989; Chhabra et al., 1989)

$$f(\alpha) = q\alpha(q) - \tau(q) \tag{8}$$

The spectrum is an inverted parabola for $c_i(\delta)$ multifractally distributed with a wider range of α values when the heterogeneity of the distribution increases. In the case of $c_i(\delta)$ monofractally distributed, α is the same for all the intervals of identical time resolution and the multifractal spectrum consists of a single point (Kravchenko et al., 1999). The extreme values in the distribution of c are associated with the lower values of $f(\alpha)$ in such a way that the high and low values in the amount of tracer particles are related to the left and right parts of the spectrum, respectively. The highest value of $f(\alpha)$ corresponds to the capacity dimension of the support (i.e. 1, when dealing with 1-D time series).

3 RESULTS

The idealized bed roughness shown in Fig. 1 was used to perform the numerical simulations, considering h/w = 1 and 0.5, with the aim of reproducing the skimming and wake interference flow regimes, respectively. In all the tests, the Reynolds number Re = 5000, the free stream velocity U = 1 m s^{-1} and the kinematic viscosity $\upsilon = 10^{-6}$ m^2/s, were kept constant. The length and time scales were $\Delta r = 0.5\times10^{-3}$ m and $\Delta t = 0.05\times10^{-3}$ s, respectively, giving a relaxation time $\eta = 0.5006$. The value of C_{smg} was 0.12 in all the simulations. The dimensions of the entire computational domain were x/h = 30 and z/h = 6 and the windward side of the first roughness element was always placed at x/h = 5. The flow was set by assigning the free stream velocity U at the inlet in such a way that $u_x = U$ and $u_z = 0$. The same values were considered for the velocity at the top of the computational domain $h_C = 6h$. Although this boundary condition was more restrictive than the rigid-lid approximation, it was chosen because of its low cost in terms of execution time. In order to apply this boundary condition, the relaxation time parameter, η, needed to be equal to 1 at these places. The so-called "porous plug" boundary condition described by Succi (2001) was used at the outlet in order to avoid the propagation of disturbances backward into the computational domain. This boundary condition works well when the outlet is not too close to the inlet as happens in the problem analyzed here, because the length of the computational domain is $l_C = 30h$. The no-slip boundary condition was applied at the roughness element walls and the flume bed by reversing all the f_i's at these sites.

The time series in the tracer transport were 2^{14} time-steps in length and they were obtained according to the following method: i) Twenty passive tracer particles were released in each time-step in the computational domain, at the source line marked in Fig. 1, once the flow was well established. ii) The amount of particles passing through the downstream boundary of the test section (Fig. 1) was determined in each time-step.

The time series simulated are shown in Fig. 2. The effects of higher streamwise and vertical turbulent intensities for the skimming flow can be seen in this figure because of the relevant presence of extreme high values in the time series of this flow regime compared to the wake interference flow. Table 1 lists the results obtained from the statistical analysis of the time series. It can be verified that the mean values (tracer particles×time-step^{-1}) are similar. However, the coefficients of variation (CV) are different as a consequence of the presence of a greater heterogeneity in the time series corresponding to the skimming flow due to higher turbulence intensity. The coefficients of skewness (CS) are positive for both turbulent regimes denoting that the right tails of the probability distributions are longer than the left ones. According to the higher value of the CS, this fact is more relevant in the case of the skimming flow.

The transfer of momentum across the shear layer at the top of the roughness elements is the origin of this single vortex inside the cavities.

The wake interference flow was fully developed for h/w = 0.5 (Fig. 3(b)). The secondary vortex inside the cavity was clearly visible, due to the absence of tracer particles at this zone, as reported Khan et al. (2005). Well-established vortices were found inside the cavities for the skimming flow. However, a more unorganized flow pattern was reproduced for the wake interference regime within the cavities except at the upstream corner

The lower the values of h/w the lower the turbulent intensities and this circumstance denotes the presence of a very weak, almost vanishing, shear layer for the wake interference regime. Thus, the interaction between the flow structures taking place outside and inside the cavities was enhanced.

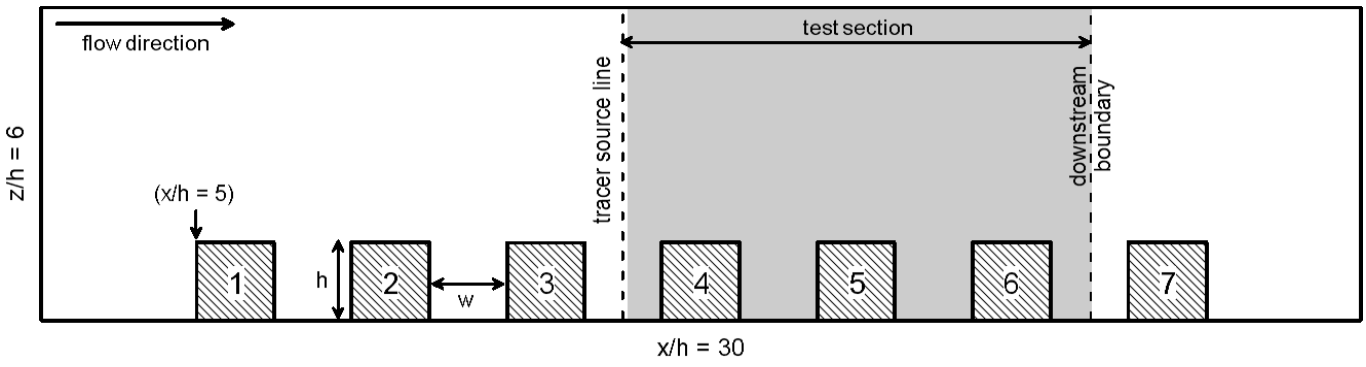

Figure 1. Scheme of the computational domain used in the simulations. The idealized bed roughness elements are marked from 1 to 7.

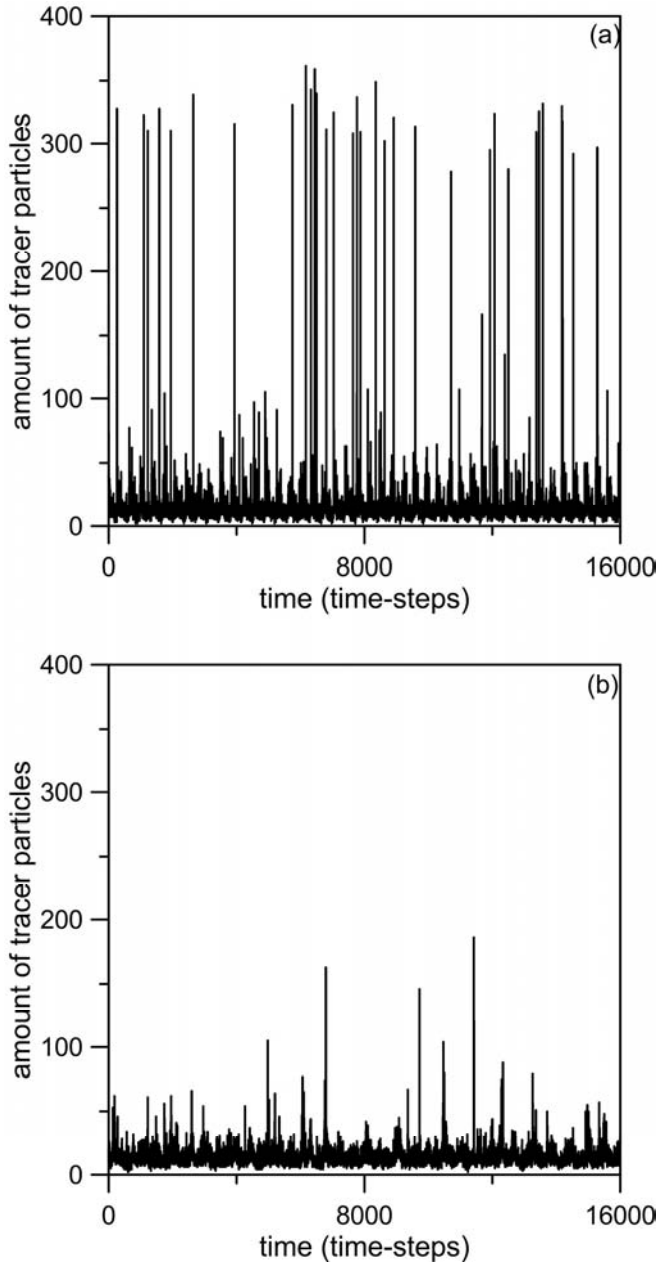

Figure 2. Simulated time series in passive tracer transport for (a) skimming and (b) wake interference flows.

In fact, the upper flow drove the secondary vortices within the cavities. The number of tracer particles was increased inside the cavities for the wake interference regime demonstrating that is associated with shear reduction at the top of the roughness elements, as observed by Khan et al. (2005).

It can be seen in Fig. 3 that the flow was less affected in the upper regions of the computational domain by the influence of the bed roughness. This fact caused the flow visualization method to reproduce paths that seem to be contour lines as a consequence of the less disturbed trajectories followed by the tracer particles. The region of influence of the bed roughness on the flow extended to $z/h \approx 3$. Cui et al. (2003) found a similar result when simulating the turbulent flow in a channel with rib roughness using LES, considering $Re = 10^4$ and applying the no-slip boundary condition at the top of the computational domain. They found that the region where the flow heavily depends on the roughness geometry extends to $z \approx 4h$.

Table 1. Statistical properties of the time series in the passive tracer transport

Flow regime	Mean	CV	CS
Skimming	14.16	1.12	14.91
Wake interference	13.96	0.49	5.07

It can be seen in Fig. 3 that the flow was less affected in the upper regions of the computational domain by the influence of the bed roughness. This fact caused the flow visualization method to reproduce paths that seem to be contour lines as a consequence of the less disturbed trajectories followed by the tracer particles. The region of influence of the bed roughness on the flow extended to $z/h \approx 3$. Cui et al. (2003) found a similar result when simulating the turbulent flow in a channel with rib roughness using LES, considering $R = 10^4$ and applying the no-slip boundary condition at the top of the computational domain. They found that the region where the flow heavily depends on the roughness geometry extends to $z \approx 4h$.

Figure 4 shows the plots of the partition functions, $\chi(q,\delta)$, versus the time resolution, that ranges from $\delta = \delta_{ini} = 2$ to $\delta = 2^{14}$ time-steps, for the tracer transport in the skimming and wake interference flows. For all the statistical orders, $q = -10$ to 10 tested at 0.5 increments, the log-transformed $\chi(q,\delta)$ can be fitted by linear regressions with the values of the coefficient of determination, r^2, ranging from 0.98 to 0.99. This fact means that the estimation of $\tau(q)$ as the slope of the linear fits can be trusted. The mass exponent functions, $\tau(q)$, were obtained from the slopes of these fits and are plotted in Fig. 5a.

Note that the $\tau(q)$ curves are convex indicating that all the time series in the tracer transport are of a multifractal nature. Figure 5b shows the multifractal spectra obtained for the tracer transport when the skimming and wake interference flows were simulated. The spectra are inverted parabolas exhibiting a longer tail to the left of the maximum value of $f(\alpha)$ in all the cases. This part of the spectra corresponds to the higher val-

ues in the amount of tracer particles, which are amplified by the positive orders $q > 0$, indicating that there was a greater heterogeneity of these values in the time series. This fact is related to the positive CS values obtained from the statistical analysis. The presence of rare high values (Fig. 2a) in the time series simulated for the skimming flow should be noted, as can be inferred from the significant number of points located at the left extreme of the spectrum. This behaviour is associated with the higher CV and CS values found for the skimming flow.

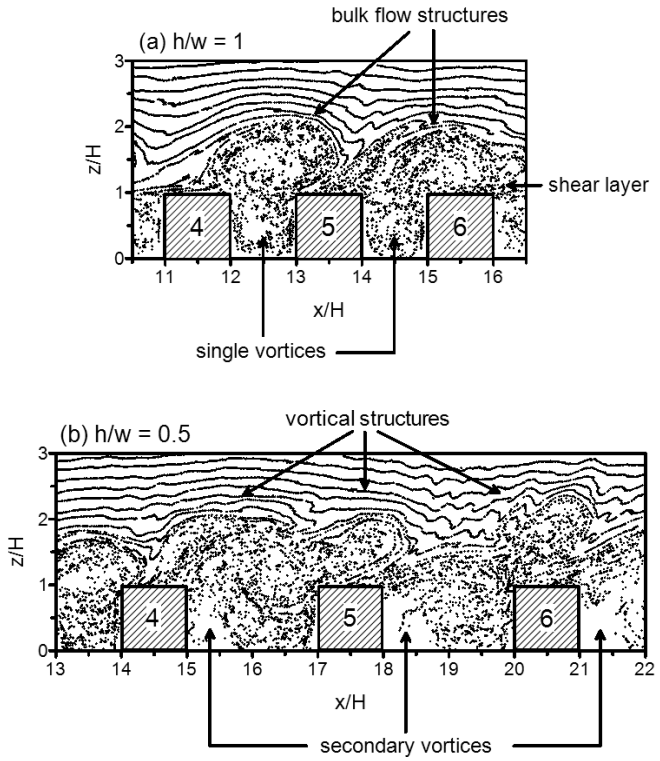

Figure 3. Flow patterns reproduced by the lattice BGK model for different aspect ratios. (a) Skimming flow (h/w = 1). (b) Wake interference flow (h/w = 0.5).

The spectrum corresponding to the wake interference flow looked sharper compared to the skimming flow case. The width of the spectrum, related to the variability in the distribution, increased as h/w became higher explaining the lower CV value detected in the time series obtained for the wake interference flow regime. The lower the values of h/w, the lower the turbulence intensities over the roughness elements, denoting the presence of a weaker shear layer for the wake interference flow.

As a consequence, the time series of the amount of tracer particles passing through the test section downstream boundary in each time-step showed less variability.

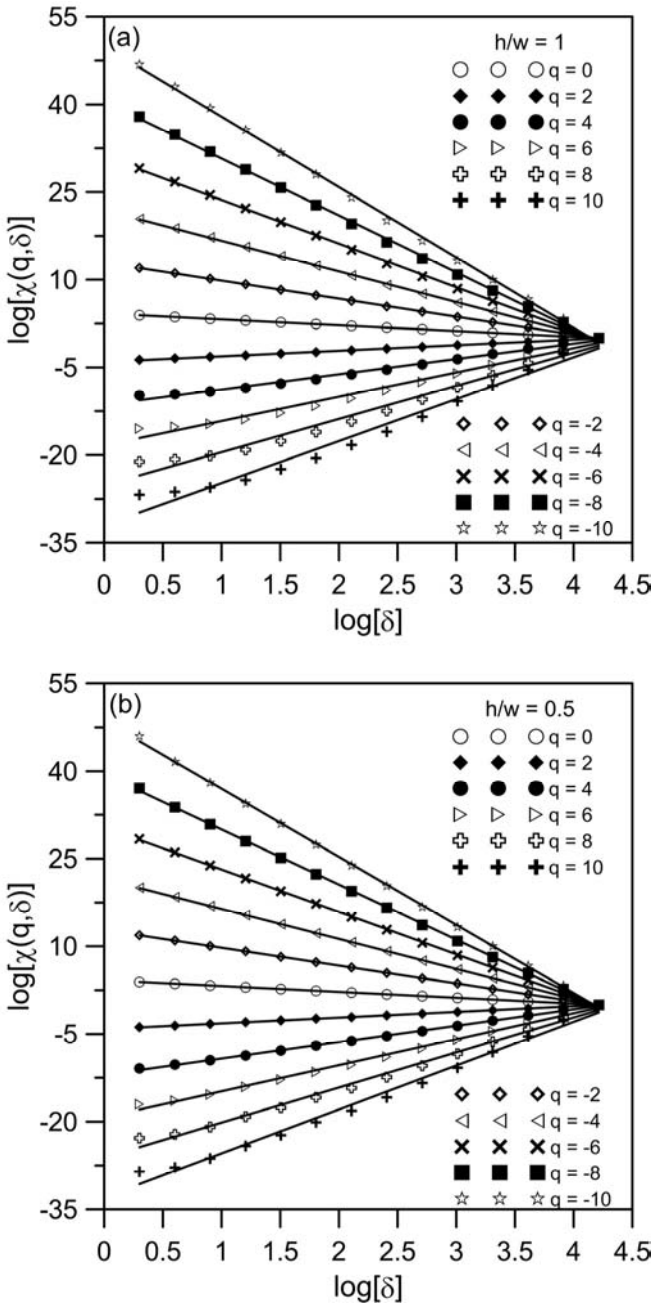

Figure 4. Log-log plots of the partition functions $\chi(q,\delta)$ versus the time resolution δ for (a) skimming and (b) wake interference flows. The mass exponent functions $\tau(q)$ were obtained from the slopes of the linear fits (solid lines) to the partition functions (symbols).

4 CONCLUSIONS

The numerical study carried out in this work demonstrates the ability of the lattice BGK model to describe the skimming and wake interference flows in the presence of an idealized bed roughness. The flow patterns and turbulent structures reproduced by the proposed lattice BGK model reasonably agree with the qualitative observations recorded in the experiments reported by Khan et al. (2005). The strange attractor multifractal formalism has been applied to describe the time se-

ries in tracer transport for the simulated flow regimes. The results obtained from the analysis of the multifractal spectra completed the information provided by the coefficients of variation and skewness. Thus, a greater heterogeneity for the high values of the time series was found for all the cases. In addition, the spectrum of the wake interference flow was sharper than the one corresponding to the skimming flow confirming a greater variability in the time series simulated for the latter flow regime. The study of the extremes of the spectra tails revealed the presence of rare high values in the time series corresponding to the skimming flow. Both the greater variability and the existence of extreme values in the tracer transport time series under the skimming flow condition, seem to be related to the increase in the turbulence intensity due to the presence of a strong shear layer on the top of the idealized bed roughness elements.

The multifractal framework has shown itself to be a suitable and efficient approach to describing the temporal structure of the tracer transport for turbulent flows in water flumes with idealized bed roughness. Based on the results reported here and taking into account that further work needs to be done, the multifractal framework can be considered as a promising tool to improve the knowledge on the pollutant and sediment turbulent dispersion in open channels.

Acknowledgments

The authors gratefully acknowledge the support of the Spanish Ministry of Science and Innovation Project AGL2009-12936-C03-02 /AGR.

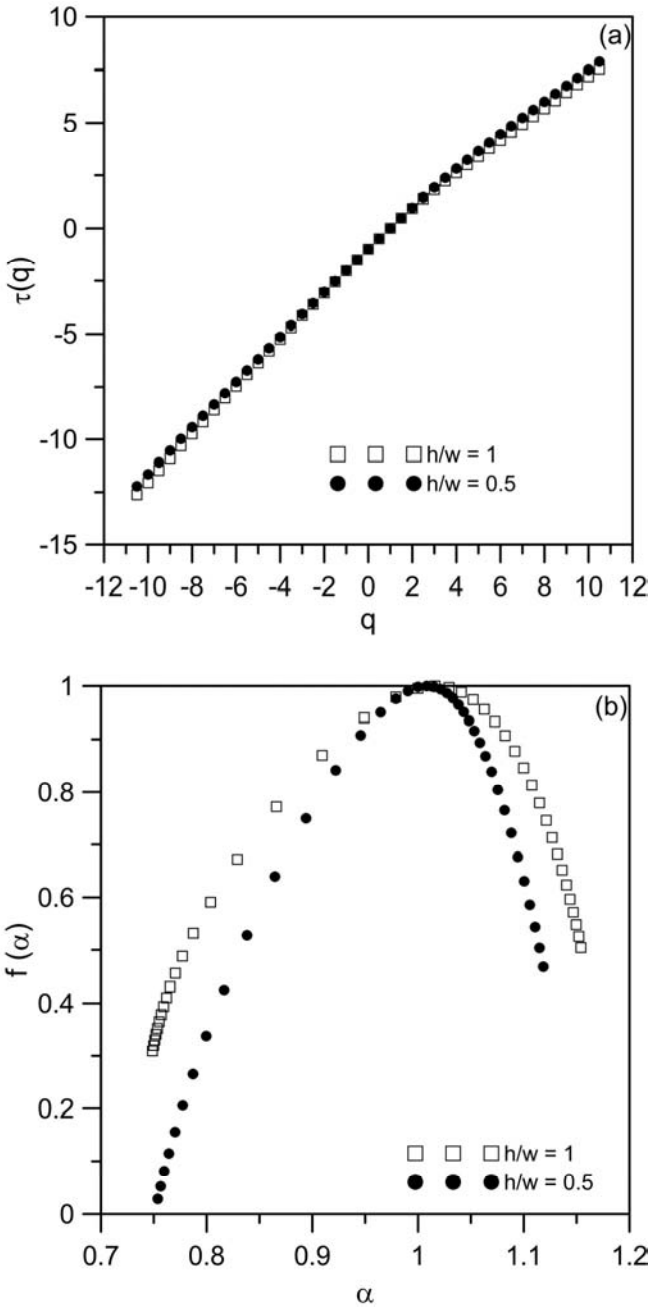

Figure 5. (a) The mass exponent functions $\tau(q)$ and (b) multifractal spectra obtained for the simulated time series in the passive tracer transport for the skimming (*h/w* =1) and wake interference (*h/w* = 0.5) flows.

REFERENCES

Chen, S., Doolen, G.D. 1998. Lattice Boltzmann method for fluid flows. Annual Review of Fluid Mechanics, 30, 329-364.

Chen, S., Wang, Z., Shan, X., Doolen, G. 1992. Lattice Boltzmann computational fluid dynamics in three dimensions. Journal of Statistical Physics, 68(3-4), 379-400.

Chhabra, A.B., Jensen, R.V. 1989. Direct determination of the $f(\alpha)$ singularity spectrum. Physical Review Letters, 62(12), 1327-1330.

Chhabra, A.B., Meneveau, C., Jensen, R.V., Sreenivasan, K.R. 1989. Direct determination of the $f(\alpha)$ singularity spectrum and its application to fully developed turbulence. Physical Review A 40(9), 5284-5294.

Chopard, B., Droz, M. 1998. Cellular automata modeling of physical systems. Cambridge University Press, Cambridge.

Cui, J., Patel, V.C., Lin, C.L. 2003. Large-eddy simulation of turbulent flow in a channel with rib roughness. International Journal of Heat and Fluid Flow, 24(3), 372-388.

Davidson, P.A. 2004. Turbulence: an introduction for scientist and engineers. Oxford University Press, New York.

Evertsz, C.J.G., Mandelbrot, B.B. 1992. Multifractal measures (Appendix B), in Peitgen H.O. et al. (Eds.), Chaos and Fractals, Springer-Verlag, New York.

Grass, A.J. 1971. Structural features of turbulent flow over smooth and rough boundaries. Journal of Fluid Mechanics, 50(2), 233-255.

Grassberger, P. 1983. Generalized dimensions of strange attractors. Physics Letters A, 97(6), 227-230.

Halsey, T.C., Jensen, M.H., Kadanoff, L.P., Procaccia, I., Shraiman, B.I. 1986. Fractal measures and their singularities: the characterization of strange sets. Physical Review A, 33(2), 1141-1151.

Hentschel, H.G.E., Procaccia, I. 1983. The infinite number of generalized dimensions of fractals and strange attractors. Physica D, 8(3), 435-444.
Hou, S., Sterling, J., Chen, S., Doolen, G.D. 1996. A Lattice subgrid model for high Reynolds number flows. Fields Institute Communications, 6, 151-166.
Khan, I.J., Simons, R.R., Grass, A.J., 2005. Effect on turbulence production due to sudden change in flow regimes. Journal of Hydraulic Research, 43(5), 549-555.
Kravchenko, A.N., Boast, C.W., Bullock, D.G. 1999. Multifractal analysis of soil spatial variability. Agronomy Journal, 91(6), 1033-1041.
Lesieur, M., Métais, O., Comte, P. 2005. Large-eddy simulations of turbulence. Cambridge University Press, Cambridge.
Morris, H.M. 1955, Flow in rough conduits. ASCE Transactions, 120 paper n.2745, 373-398.
Perry, A.E., Joubert, P.N. 1963. Rough-wall boundary layers in adverse pressure gradients. Journal of Fluid Mechanics, 17(2), 193-211.
Pope, S.B. 2000. Turbulent flows. Cambridge University Press, Cambridge.
Qian, Y.H., D'Humieres, D., Lallemand, P. 1992. Lattice BGK models for Navier-Stokes equation. Europhysics Letters, 17(6bis), 479-484.
Succi, S. 2001. The lattice Boltzmann equation for fluid dynamics and beyond. Oxford University Press, Oxford.
Xia, J., Leung, Y.C. 2001. Pollutant dispersion in urban street canopies. Atmospheric Environment, 35(11), 2033-2043.
Zhou, J.G. 2002. A lattice Boltzmann model for the shallow water equations with turbulence modelling. International Journal of Modern Physics C, 13(8), 1135-1150.